Environmental Pollution 247 (2019) 146–154

Contents lists available at ScienceDirect

Environmental Pollution

journal homepage: www.elsevier.com/locate/envpol

$[SnS_4]^{4-}$ clusters modified MgAl-LDH composites for mercury ions removal from acid wastewater☆

Lihong Chen [a], Haomiao Xu [a, *], Jiangkun Xie [a, b], Xiaoshuang Liu [a], Yong Yuan [a], Ping Liu [a], Zan Qu [a], Naiqiang Yan [a]

[a] School of Environmental Science and Engineering, Shanghai Jiao Tong University, Shanghai, 200240, PR China
[b] Shanghai Institute of Pollution Control and Ecological Security, Shanghai, 200092, PR China

ARTICLE INFO

Article history:
Received 12 August 2018
Received in revised form
4 December 2018
Accepted 4 December 2018
Available online 4 January 2019

Keywords:
$SnS_4]^{4-}$ cluster
Hg^{2+} ions removal
Acid wastewater
Layered double hydroxides

ABSTRACT

The high acidity of mercury ions (Hg^{2+}) contained wastewater can complicate its safe disposal. MgAl-LDHs supported $[SnS_4]^{4-}$ clusters were synthesized for Hg^{2+} removal from acid wastewater. The active sites of $[SnS_4]^{4-}$ clusters were inserted into the interlayers of MgAl-LDHs using an ion-exchange method. The experimental results indicated that $[SnS_4]^{4-}$/MgAl-LDHs composite can obtain higher than 99% Hg^{2+} removal efficiency under low pH values. The maximum mercury adsorption capacity is 360.6 mg g^{-1}. It indicated that $[SnS_4]^{4-}$ clusters were the primary active sites for mercury uptake, existing as stable $Hg_2(SnS_4)$ on the surface of the composite. Under low pH values, such a composite seems like a "net" for $HgSO_4$ molecules, exhibiting great potential for mercury removal from acid solutions. Moreover, the co-exist metal ions such as Zn^{2+}, Na^{+}, Cd^{2+}, Cr^{3+}, Pb^{2+}, Co^{2+}, and Ni^{2+} have no significant influences on Hg^{2+} removal. The adsorption isotherms and kinetics were also studied, indicating that the adsorption mechanism follows a monolayer chemical adsorption model. The $[SnS_4]^{4-}$/MgAl-LDHs composite exhibits a great potential for Hg^{2+} removal from acid wastewater.

© 2019 Elsevier Ltd. All rights reserved.

1. Introduction

Mercury, with the features of high toxicity, low volatility, easy mobility and bioaccumulation, has negative effects on human's health and ecosystem (Jia et al., 2017; Ke et al., 2012; Zhi et al., 2016). The natural and anthropogenic sources such as volcanic eruption, domestic activities, and some mercury containing products can release mercury into aqueous environment (United Nations Environment Programme (UNEP), 2013; Tahmasebi et al., 2014; Trasande et al., 2016). Mercury ions (Hg^{2+}) in aqueous environment are considered as one of the most toxic and dangerous pollutants (Hargreaves et al., 2016; Xue et al., 2016). The increasing use of mercury in some industrial processes and products can result in a deterioration in aqueous environment. Therefore, the elimination of mercury from aqueous media has received widespread attention in recent years (Sun et al., 2014).

Large quantities of mercury emitted from various industrial sources (Hassan et al., 2018; Kumari, 2011). Mercury contained wastewater from the non-ferrous metal smelting process is a typical one (Coleman et al., 1980). In general, the gaseous elemental mercury (Hg^0) and the oxidized mercury (Hg^{2+}) are trapped by wet scrubber device (Xu et al., 2015; Xu et al., 2018). In this process, large amount of sulfur dioxide in the smelting gas will also enter into the wastewater, forming the mercury-contained acid wastewater (Ma et al., 2014a). Recent study has shown that a polymer material containing TOMAC as an extractant exhibits high mercury selectivity under acidic conditions (pH = 1.0) in the presence of chloride ions (Borreguero et al., 2018). Mercury removal from acidic wastewater has been and will continue being the focus of many researches.

Numerous methods have been applied for the removal of heavy metal ions from wastewater such as chemical precipitation, ion-exchange, adsorption, membrane separation, and electrochemical treatment (Fang et al., 2018; Gong et al., 2014; Ma et al., 2017; Xu et al., 2016a; Zhao et al., 2016). Chemical precipitation was the widely used method for mercury ions removal. However, it needs to adjust pH to realize the precipitation. Ion-exchange can get high ions removal efficiency. However, most of ions exchange resins have low selectively for Hg^{2+}. For membrane separation method,

☆ This paper has been recommended for acceptance by Joerg Rinklebe

* Corresponding author.
E-mail address: xuhaomiao@sjtu.edu.cn (H. Xu).

https://doi.org/10.1016/j.envpol.2018.12.009
0269-7491/© 2019 Elsevier Ltd. All rights reserved.

the problem of membrane fouling is difficult to be solved. Also, the high price of electrochemical treatment and membrane method limited their use widely. Among these methods, adsorption method, with the advantages of operation simplicity, high removal efficiency and high economic benefit, has been proved to be one of the most promising methods (Abu-Danso et al., 2018; Sun et al., 2017). Various types of adsorbents have developed for the uptake of mercury. Qu et al. reported a novel sorbent, zinc sulfide nanocrystals, which can efficiently remove over 99.9% Hg^{2+} in only 1 min under pH 5.5 and room temperature conditions (Qu et al., 2014). Ma et al. observed that the MoS_4-LDH exhibits an outstanding Hg^{2+} removal efficiency (room temperature; pH = 3.0; reaction time, 24 h) (Ma et al., 2017). However, most of the reported adsorbents are strongly affected by the fluctuation of solution's pH value. The high acidity of wastewaters containing mercury ions (Hg^{2+}) can complicate its safe disposal (Chu et al., 2015; Fakhri, 2015). In addition, wastewater from smelting process is a challenge due to the low pH values as well as the complex compositions (containing copper, zinc, lead, and other heavy metals). Therefore, an appropriate adsorbent should have high adsorption affinity for mercury in acidic wastewater (Muliwa et al., 2017).

Mercury is a soft Lewis acid while sulfur shows a high bonding affinity to mercury (Gong et al., 2012). Sulfur-based materials are recognized as promising materials for mercury remediation. Polymeric sulfur, mineral sulfides, sulfur-containing framework structural materials, chalcogenide clusters and chalcogels are widely reported (Ali and Mazumder, 2018; Barth et al., 2013; Jawad et al., 2017; K et al., 2002; Sajjadi et al., 2018; Shafaei-Fallah et al., 2011; Shim et al., 2013; Yuhas et al., 2011). Among these materials, pure sulfur power suffers slow reaction rate toward mercury. Mineral sulfides are restricted for application due to low mercury capacities. However, chalcogenide cluster exposes more surface sulfur-active sites and they exhibit an open framework and pore structures. It was reported that $[Sn_2S_6]^{4-}$, $[SnS_4]^{4-}$ and other chalcogenide clusters exhibit high affinity toward soft heavy-metal ions (Oh et al., 2011). An ideal support for chalcogenide clusters is also of significant when used for adsorption. Layered double hydroxides (LDHs) is one kind of mineral consisting of positively charged host layers and counter-anions in the interlayer space (Zhang et al., 2017; Gu et al., 2018). Their layered structure and anion exchange capacity make them being widely applied in the fields of catalysis, nano-materials, and adsorption (Yu et al., 2018). Sulfur clusters can enter into the interlayered structure using an ion-exchange method. Hence, the employment of LDHs intercalated with chalcogenide cluster could provide considerable economic and environmental benefits for the treatment of mercury-containing wastewater.

Herein, in this work, mixed solution of sulfuric acid and mercury sulfate was chosen as the target mercury-contained acid wastewater. $[SnS_4]^{4-}$ cluster modified MgAl-LDH composite was prepared using an ion-exchange method between MgAl-LDHs and $[SnS_4]^{4-}$ clusters. This study mainly focuses on the investigation of the performance and mechanisms of mercury removal from acidic wastewater using $[SnS_4]^{4-}$/MgAl-LDH composite. Batch adsorption experiments were performed under various operating conditions. The adsorption isotherms and kinetics were also studied.

2. Methods and materials

2.1. Chemicals

The main reagents used in this study are sodium sulfide (Aldrich, >99%), tin chloride pentahydrate (Aldrich, >99%), methanol (>99%), ethanol (EtOH, >99%), magnesium nitrate hexahydrate (>99%), zinc sulfate heptahydrate (>99.5%), sodium sulfate anhydrous (>99%), sodium hydroxide (>99.9%), copper sulfate pentahydrate (>99%), aluminum nitrate (>99%), cobalt nitrate hexahydrate (>99%), lead nitrate, nickel nitrate hexahydrate (>99%), hydrochloric acid (37%), sulfuric acid (95–98%), mercury sulfate (AR, 99%), mercury chloride (>99%), and methanol (>99.9%).

2.2. Synthesis of materials

2.2.1. Synthesis of Na_4SnS_4

Firstly, precursor Na_4SnS_4 was prepared based on previous literature (Oh et al., 2011). 120 mmol of sodium sulfide ($Na_2S \cdot 9H_2O$) was dissolved in 100 mL deionized distilled water. 30 mmol of tin tetrachloride ($SnCl_4 \cdot 5H_2O$) was added into 50 mL deionized distilled water. After dissolution, $SnCl_4 \cdot 5H_2O$ solution was added dropwise to the $Na_2S \cdot 9H_2O$ solution with continuous stirring. 400 mL of methanol was added into the mixed solution and kept stirring at 45 °C for 8 h. Then, the solution was stored in a refrigerator for 2 d to form precipitated white crystals of Na_4SnS_4. Afterwards, the sample was washed with ethanol and dried in a vacuum oven at 65 °C for 24 h.

2.2.2. Synthesis of MgAl-LDHs

The MgAl-LDH in the nitrate form was synthesized using a co-precipitation method (Gonzalez Rodriguez et al., 2017). The molar ratio of magnesium nitrate ($Mg(NO_3)_2 \cdot 6H_2O$) to aluminum nitrate ($Al(NO_3)_3 \cdot 9H_2O$) was set as 2: 1. The mixture was dissolved in ultrapure water and sodium hydroxide (NaOH) solution was used to adjust the pH to 10, and then kept stirring for 10 h using nitrogen protection. The precipitates were centrifuged and rinsed several times with deionized water and ethanol. The product finally was dried at 80 °C for further use.

2.2.3. Synthesis of $[SnS_4]^{4-}$/MgAl-LDH composite

The $[SnS_4]^{4-}$/MgAl-LDH composites were prepared using Na_4SnS_4 and MgAl-LDHs with three different mass ratio of 1:3, 1:6, and 1:10 (marked as R-3, R-6, and R-10). And seven kinds of $[SnS_4]^{4-}$/MgAl-LDH with different Na_4SnS_4 content (25%, 14%, 9%, 7%, 5%, 3%, 1%) were also synthesized. The ion-exchange reaction equation was as follows.

$$Mg_{0.78}Al_{0.39}(OH)_{2.5}(NO_3)_{0.23} + 0.0575Na_4SnS_4$$

$$\rightarrow Mg_{0.78}Al_{0.39}(OH)_{2.5}(SnS_4)_{0.0575} + 0.23NaNO_3 \quad (1)$$

For the ratio of 1:3, 1.5 g MgAl-LDHs was dissolved in 100 mL deionized water with ultrasonic treatment for 2 h. Then 0.5 g Na_4SnS_4 was added and kept stirring for 12 h (300 r min^{-1}). The resulting mixture were filtered, washed with ethanol, and dried at 80 °C for 12 h. Finally, the light yellow solid is the adsorbent required for this study. And the yield of as-prepared samples is 1.12 g, which is about 75% of the theoretical yield.

2.3. Characterization

X-ray diffraction (XRD) patterns were recorded by a Shimadzu XRD-6100 diffractometer with Cu-Kα radiation. The data were recorded at a scan rate of 10 deg·min^{-1} in the 2θ range from 10 to 80°. The surface areas of materials were detected via Brunauer-Emmett-Teller (BET) method by N_2 gas sorption on a surface area and pore size analyzer (Quantachrome Instruments NOVA 2200e). Functional groups of adsorbent were identified by infrared spectra analysis (FT-IR) with 64 scans in range of 4000–500 cm^{-1}. The component's content of solution after the adsorption reaction was analyzed by inductively coupled plasma-atomic emission spectroscopy (ICP-AES) (iCAP7600, America). The surface morphologies of sorbents were characterized by field emission scanning electron

microscopy (SEM, JSM-7001F) and transmission electron microscope (TEM, JEM-2100F). X-ray photoelectron spectroscopy (XPS) results were recorded with an Ultra DLD (Shimadzu-Kratos) spectrometer with Al Kα as the excitation source, and the C 1s line at 284.6 eV was used as a reference for the binding energy calibration.

2.4. Experiments for Hg^{2+} removal

This work is aiming to develop an adsorbent for mercury removal from acidic wastewater produced by non-ferrous smelting process. Table S1 summarizes the targeted wastewater quality. To explore the Hg^{2+} removal performances of the as-prepared adsorbent, batch adsorption experiments were conducted. We firstly investigate the Hg^{2+} removal performances under mercury chloride ($HgCl_2$) and mercury sulfate ($HgSO_4$) solutions over $[SnS_4]^{4-}$/MgAl-LDH composite. The initial pH value of both solutions were set as about 2.0. To further investigate the Hg^{2+} removal efficiencies of adsorbents from sulfuric acidic wastewater, 50 mg $[SnS_4]^{4-}$/MgAl-LDH composite (R-3) was added into 50 mL of $HgSO_4$–H_2SO_4 solution with stirring (300 r min^{-1}) at room temperature. The initial Hg^{2+} concentrations of simulated solution ranged from 289.6 mg L^{-1} to 5.28 mg L^{-1}. Besides, adsorption experiments to investigate the influence of pH, mass ratio and co-exist ions were conducted separately using $[SnS_4]^{4-}$/MgAl-LDH composite (R-3). For all adsorption experiments, equal volumes of sample were taken with disposable syringes at the target reaction time then filtered through a filter (pore size: 220 nm). Each sample solution was analyzed twice using a mercury analyzer (RA915, St. Petersburg, Russia) to measure the concentration of Hg^{2+} and to calculate Hg^{2+} removal efficiency. The Hg^{2+} removal efficiency was calculated based on the following equation:

$$\eta = \frac{C_0 - C_t}{C_0} \times 100\% \tag{2}$$

where C_t and C_0 represent the initial and instantaneous concentrations of mercury ions, respectively.

Batch adsorption isotherm experiments were carried out by adding 50.0 mg of sorbent (R-3) into 100 mL of mercury solution with an initial concentration ranging from 5.0 to 300.0 mg L^{-1}. In all experiments, the pH of the mixture was adjusted to about 2.0 with H_2SO_4. The reaction time was 24 h to reach adsorption equilibrium. The removal capacity under equilibrium conditions was calculated according to eq (3):

$$Q_e = \frac{(C_0 - C_e) \times V}{m} \tag{3}$$

where C_0 and C_e are the initial and equilibrium concentrations of mercury ions (mg L^{-1}), respectively. V is the volume of the reaction solution (L), and m denotes the amount of the used $[SnS_4]^{4-}$/MgAl-LDH (g).

The classical Langmuir model (3) and Freundlich model (4) were used to simulate the adsorption isotherm. The two typical adsorption isotherm models can be expressed as the below equations (Zhang et al., 2018):

Langmuir model:

$$\frac{Ce}{Qe} = \frac{Ce}{Qmax} + \frac{1}{Qmax \times K_L} \tag{4}$$

Freundlich model:

$$LogQe = logK_F + 1/n \times logCe \tag{5}$$

where Ce (mg L^{-1}) is the equilibrium concentration of mercury ions remained in solution, Qe (mg g^{-1}) is the amount of mercury ions adsorbed after equilibrium, Qmax is the saturated adsorption capacity (mg g^{-1}), K_L and K_F refer to the affinity parameter of the Langmuir and Freundlich adsorption constants, respectively, and $1/n$ is Freundlich constant related to adsorption intensity parameter.

The adsorption kinetic experiments were carried out with an initial Hg^{2+} concentration of 10 mg L^{-1}, 50 mg L^{-1}, and 100 mg L^{-1} at an initial pH of 2.0 for 60 min reaction. The dose of adsorbent was 50 mg. The experiment data was analyzed to interpret the adsorption dynamics based on pseudo-first-order model, pseudo-second-order model, and internal diffusion kinetic model. These kinetics models are given as follows (Amiri et al., 2018; Hafeznezami et al., 2016):

Pseudo-first-order kinetic model:

$$log(Qe - Qt) = logQe + k_1 t/2.303 \tag{6}$$

Pseudo-second-order kinetic model:

$$t/Qt = 1\Big/\left(k_2 Qe^2\right) + t/Qe \tag{7}$$

Internal diffusion model:

$$Qt = k_i t^{0.5} \tag{8}$$

where Qe represents the equilibrium adsorption capacity (mg g^{-1}), Qt is the amount of metal ions adsorbed at time t (mg g^{-1}), k_1 (min^{-1}) and k_2 (g mg^{-1} min^{-1}) are adsorption rate constant of pseudo-first-order and pseudo-second-order model, respectively. k_i (g mg^{-1} $min^{-0.5}$) is the internal diffusion rate constant.

3. Results & discussion

3.1. Characterization of as-prepared materials

XRD is selected to investigate the crystal structure of as-prepared adsorbents. The XRD patterns of MgAl-LDH, $[SnS_4]^{4-}$/MgAl-LDH and spent $[SnS_4]^{4-}$/MgAl-LDH samples are presented in Fig. 1. The XRD pattern of MgAl-LDH sample consists seven characteristic reflection peaks at $2\theta = 12°$, 23°, 34.5°, 38.4°, 45.8°, 60.5° and 61.8° which can be indexed to (003), (006), (012), and (015)

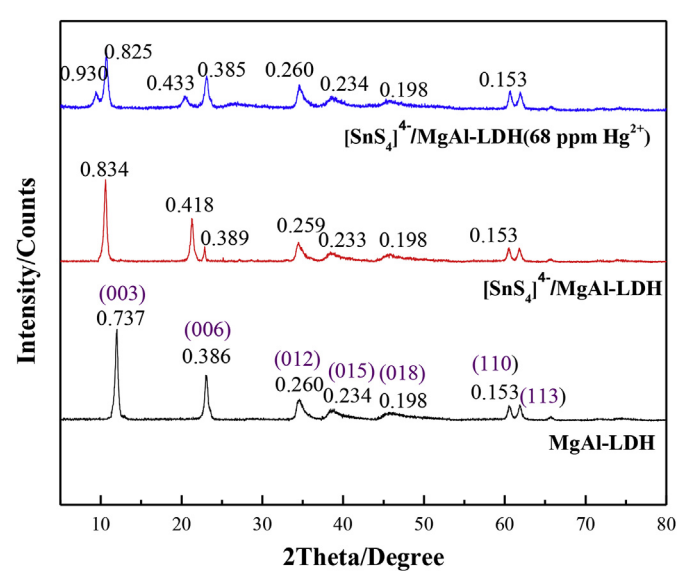

Fig. 1. XRD patterns (crystal form and structure) of MgAl-LDH, $[SnS_4]^{4-}$/MgAl-LDH and $[SnS_4]^{4-}$/MgAl-LDH samples after adsorption of mercury ions (68 ppm).

phases of Mg–Al hydrotalcite (JCPDS 35–0965), and (018), (110) and (113) phases of takovite (JCPDS 15–0087), respectively (Lei et al., 2017). Compared with MgAl-LDH, the as-prepared $[SnS_4]^{4-}$/MgAl-LDH had a larger basal spacing of 0.834 nm, indicating that larger $[SnS_4]^{4-}$ groups had been introduced into the interlayer space. The peaks at $2\theta = 10.6°$, 21.2° and 22.8° indicating a layered phase, we postulated that the weakened reflection at 22.8° compared to the stronger reflection at 21.2° results from the heavier nature of $[SnS_4]^{4-}$ groups and stronger scattering property than NO_3^- groups.

The FT-IR spectra of Na_4SnS_4, MgAl-LDH, fresh $[SnS_4]^{4-}$/MgAl-LDH and spent $[SnS_4]^{4-}$/MgAl-LDH samples are shown in Fig. S1. From the spectra, there are several representative regions: O–H stretching region (3500-3000 cm^{-1} and 1500-1750 cm^{-1}) for each sample. The absorption bands at 3395, and 1637 cm^{-1} are assigned to the O–H stretching vibrations of the hydroxyl groups in the interlayer and surface water molecules, respectively. In the spectrum of SnS_4-LDH, a strong band appearing at 1349 cm^{-1} which was corresponded to the NO_3^- of the MgAl-LDH diminished, suggesting that the exchange of $[SnS_4]^{4-}$ with NO_3^-. And the peak at 1349 cm^{-1} for Na_4SnS_4 is contributed to thiosulfate, a by-product formed by the oxidation of sodium sulfide during the synthesis of Na_4SnS_4. This peak disappeared in the spent sample because sodium thiosulfate was dissolved in the solution during the adsorption process.

As shown in Fig. S2, the SEM and TEM images of $[SnS_4]^{4-}$/MgAl-LDH verified the adsorbent had layered structure with hexagonal morphology. In addition, such a structure can be stable under acidic condition. Furthermore, the EDS results of $[SnS_4]^{4-}$/MgAl-LDH (Fig. S3) confirmed that $[SnS_4]^{4-}$ clusters were successfully introduced into MgAl-LDH. As shown in Table S2, the BET surface areas, pore volume, and pore diameter of precursors of as-prepared adsorbents were tested. $[SnS_4]^{4-}$/MgAl-LDH had a surface area of 74.713 $m^2\,g^{-1}$, which was larger than that of MgAl-LDH and Na_4SnS_4 due to the larger pore diameter and pore volume.

According to the characterization results, $[SnS_4]^{4-}$ clusters were introduced into MgAl-LDH layers using the ion-exchange method. An interlayer structure can enlarge the surface area of $[SnS_4]^{4-}$/MgAl-LDH composites. Such a structure could be beneficial for mercury ions stabilization on its interlayered surface.

3.2. Hg^{2+} removal performances with $[SnS_4]^{4-}$/MgAl-LDH composite

3.2.1. Comparison of Hg^{2+} removal in different acid conditions

Mercury often existed as $HgCl_2$ and $HgSO_4$ under sulfuric acid or hydrochloric acid contained wastewater. As shown in Fig. S4, we firstly investigate the Hg^{2+} removal performances under these two acid conditions. The results indicated that $[SnS_4]^{4-}$/MgAl-LDH composite showed good Hg^{2+} removal efficiencies in both conditions.

3.2.2. Effect of initial mercury concentration on Hg^{2+} removal

Because for non-ferrous smelting plants, Hg^{2+} often coexist with H_2SO_4, our experiments mostly focus on Hg^{2+} in sulfuric acid solution. As shown in Fig. 2(a), the Hg^{2+} removal displayed a high initial efficiency within 5 min (>99%, except 289.6 mg L^{-1}) and then slowly reached an equilibrium. Even in the case of high concentration of Hg^{2+} (up to 300 mg L^{-1}), the removal efficiency in 1 h can still reach about 99%.

3.2.3. Effect of mass ratio of $[SnS_4]^{4-}$ to MgAl-LDH on Hg^{2+} removal

Three materials with different mass ratio of Na_4SnS_4 and MgAl-LDHs (R-3, R-6 and R-10) were tested to observe whether the ratio would affect the Hg^{2+} removal performance. From Fig. S5, it was shown that under the condition of low Hg^{2+} concentration, Hg^{2+} removal remains almost the same regardless the mass ratio of $[SnS_4]^{4-}$ to MgAl-LDH.

3.2.4. Effects of co-existed ions on Hg^{2+} removal

Several other co-existed ions, such as Pb^{2+}, Cd^{2+}, Cr^{3+}, Zn^{2+}, Cu^{2+}, Na^+, Co^{2+}, and Ni^{2+} were added into $HgSO_4$–H_2SO_4 solution respectively to investigate the influence of co-existed ions on Hg^{2+} removal. As shown in Fig. 2(b), although the presence of Cu^{2+} and Cl^- decreased the Hg^{2+} removal rate, the Hg^{2+} removal efficiency is still maintained 99% in 1 h. In addition, there are no obvious decrease in removal efficiencies when other metal cations exist in the solution. It also demonstrated that the degree of ionization of mercury ions had effect on removal rate through the comparison of metal chloride and metal nitrate (Fig. 2(c)). Moreover, the research of the source of mercury ions and the solution for dissolution was carried out, which demonstrated that Cl^- had a certain influence on removal thoroughness according to Fig. S6. The explanation is that mercury sulfate is a strong electrolyte while mercury chloride is a weak electrolyte (Alcázar et al., 2015). This experiment was also applied to get clear removal ability of $[SnS_4]^{4-}$/MgAl-LDH composite for other metal ions. Comparatively good affinity for Pb^{2+}, Cu^{2+}, Cr^{3+} was got by this adsorbent as suggested by results (Fig. S7). The removal efficiencies were 99.3%, 90.2% and 79.9%, respectively.

3.2.5. Effect of initial pH value on Hg^{2+} removal

As shown in Fig. 3, the Hg^{2+} removal efficiencies of $[SnS_4]^{4-}$/MgAl-LDH composite decreased with the increase of pH values. Higher than 99% of Hg^{2+} was extracted from its initial solution within 1 h as the pH value was lower than 4.0. Especially, when the pH values were 1.0–3.0, the Hg^{2+} removal efficiencies can reach about 100%. pH affects ionization of the functional groups on an adsorbent surface as well as the speciation of ions in the solution (Li et al., 2010). And $HgSO_4$ is an ionic compound that is insoluble in water but soluble in acid solution. When the pH was gradually increasing, the main mercury species were $Hg(OH)_2$ (Sajjadi et al., 2018). Similarly, Xu et al. found that $Hg(OH)_2°$ became the predominant species according to the speciation model MINTEQ software (Xu et al., 2016b). Therefore, under lower pH value condition, the dissociation of $HgSO_4$ is more complete then mercury ions are more easily adsorbed by the adsorbent. Meanwhile, an undesirable removal efficiency was got at higher pH value. With the pH continues increasing, the $Hg(OH)_2$ and/or $Hg(OH)_3^-$ and $Hg(OH)_4^{2-}$ were the predominant species, which resulted in the adsorption capacity of Hg^{2+} decreasing. As pH continued to increase, the hydroxide species were formed as following reactions (Shadbad et al., 2011):

$$Hg^{2+} + 2OH^- \rightarrow Hg(OH)_2 \quad K_{sp} = 3.6 \times 10^{-26}$$

$$Hg(OH)_2 + OH^- \rightarrow Hg(OH)_3^- \quad LogK_1 = 10.6$$

$$Hg(OH)_3^- + OH^- \rightarrow Hg(OH)_4^{2-} \quad LogK_2 = 11.2$$

We have compared the Hg^{2+} removal performance using mercury chloride and mercury sulfate, and there is a difference between the Hg^{2+} removal efficiency. Scientifically, mercury sulfate is a strong electrolyte, while mercury chloride is a weak electrolyte. For mercury sulfate, the optimal pH value was under 3.0. The pH of metal ions solutions was regarded as one of the most important factors for the reason that it not only enhanced the binding sites by protonation in acid solution, but also influenced the adsorbent performances by affecting the surface charges and dissociation of mercury sulfate. These results implied that $[SnS_4]^{4-}$/MgAl-LDH could be employed to treat the acid wastewater efficiently.

The Hg^{2+} concentrations of the solution samples at the pH

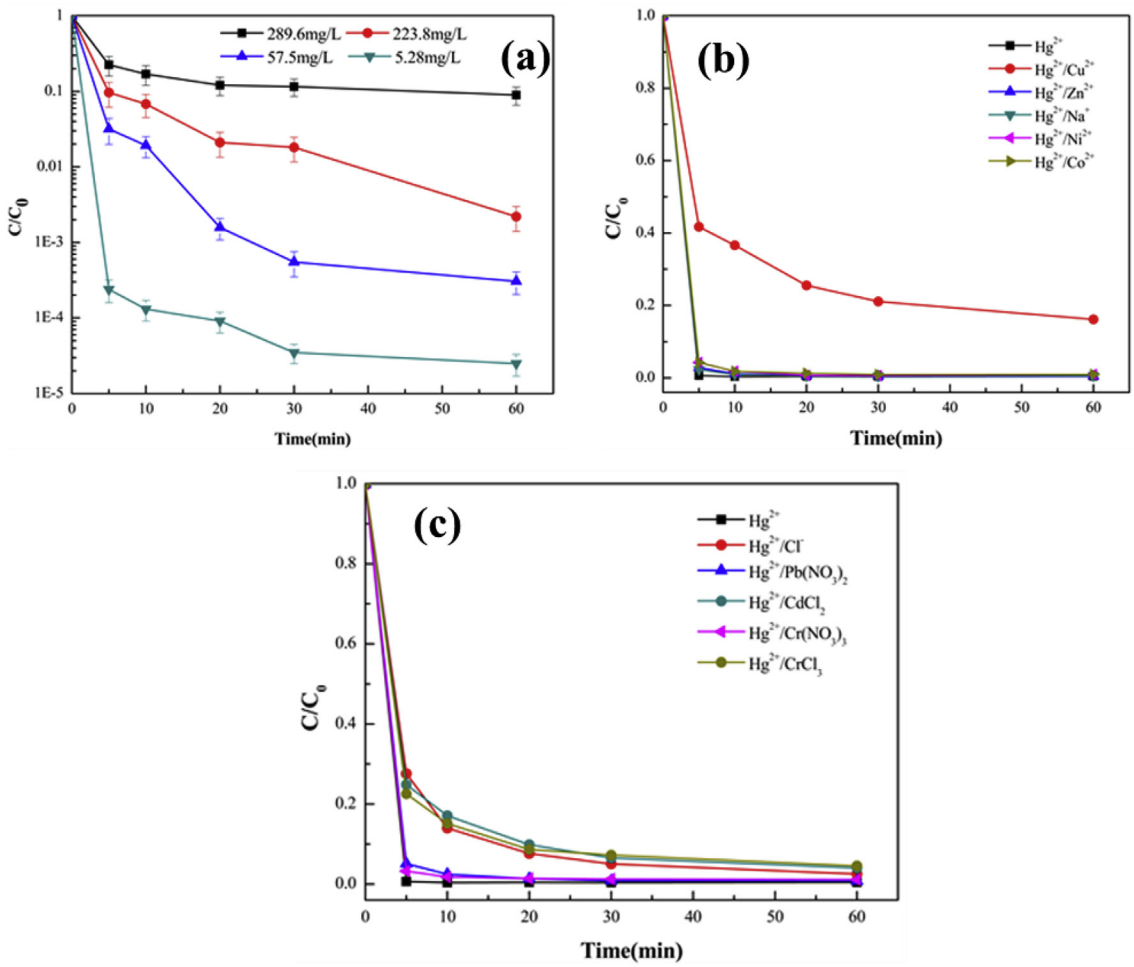

Fig. 2. (a) The influence of initial mercury concentration on Hg^{2+} removal (50 mg $[SnS_4]^{4-}$/MgAl-LDH, 50 mL solution, pH~2.0, room temperature). (b) The influence of Cu^{2+}, Zn^{2+}, Na^{+}, Ni^{2+}, Co^{2+}, and (c) $Pb(NO_3)_2$, $CdCl_2$, $Cr(NO_3)_3$, $CrCl_3$ on Hg^{2+} removal (50 mg $[SnS_4]^{4-}$/MgAl-LDH, 100 mL solution,1 mM metal ions, pH~2.0, room temperature).

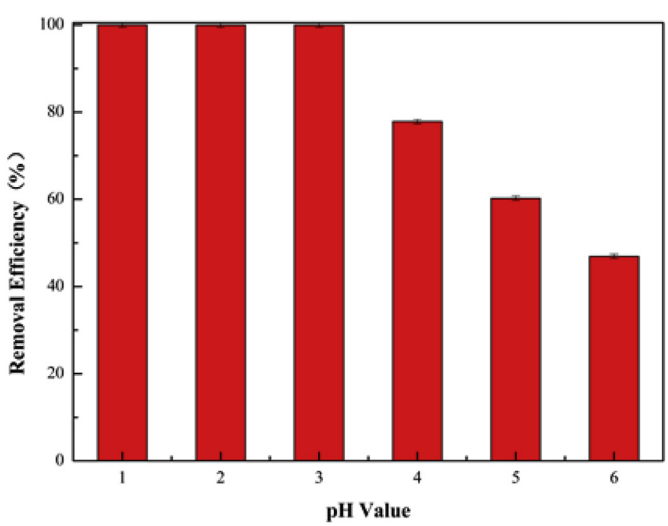

Fig. 3. Effects of pH value on Hg^{2+} removal efficiency (50 mg $[SnS_4]^{4-}$/MgAl-LDH, 100 mL solution, 67 ppm Hg^{2+}, pH~2.0, room temperature).

values of 1 and 4 were analyzed using ICP-AES, and the results were shown in Table S3. It can be seen that the Hg^{2+} concentration decreased sharply in 5 min when the pH value was 1.0. Comparatively, at pH value of 4, the Hg^{2+} removal rate decreased. Furthermore, because pH changes little before and after adsorption (Table S4), we can postulate that the alkalinity of the composite has almost no effect on the pH value of the solution. In addition, the Sn^{2+} concentration detected had no apparent changes during the course of reaction (Table S4), this indicates that $[SnS_4]^{4-}$ clusters stably coexisted with MgAl-LDH. The Hg^{2+} removal efficiency was much higher under lower pH value due to the still stable adsorption of mercury with $[SnS_4]^{4-}$ clusters. Moreover, the leaching out of Sn and Al species is little after the $[SnS_4]^{4-}$/MgAl-LDH treated by HCl solution (Table S5), indicating that the adsorbent is relatively non-toxic for wastewater treatment.

3.3. *Mechanisms of Hg^{2+} removal by $[SnS_4]^{4-}$/MgAl-LDH composite*

3.3.1. *Adsorption isotherms, uptake capacity, and adsorption kinetics*

The reaction kinetics, adsorption capacities and isotherms are evaluated to get a better understanding of the Hg^{2+} removal mechanism. The uptake capacity of $[SnS_4]^{4-}$/MgAl-LDH composite (R-3) for the Hg^{2+} ions was analyzed by the equilibrium adsorption isotherm. As shown in Fig. 4(a), the adsorption capacity increased with the increasing of Hg^{2+} equilibrium concentration and then reached the maximum. The saturated adsorption capacity of $[SnS_4]^{4-}$/MgAl-LDH composite calculated from the data was up to 360.6 mg g^{-1}, which was compared with reported Fe–MoS_4 LDH, MoS_4 LDH, and S_2-LDH (582 mg g^{-1}, 500 mg g^{-1}, and 686 mg g^{-1},

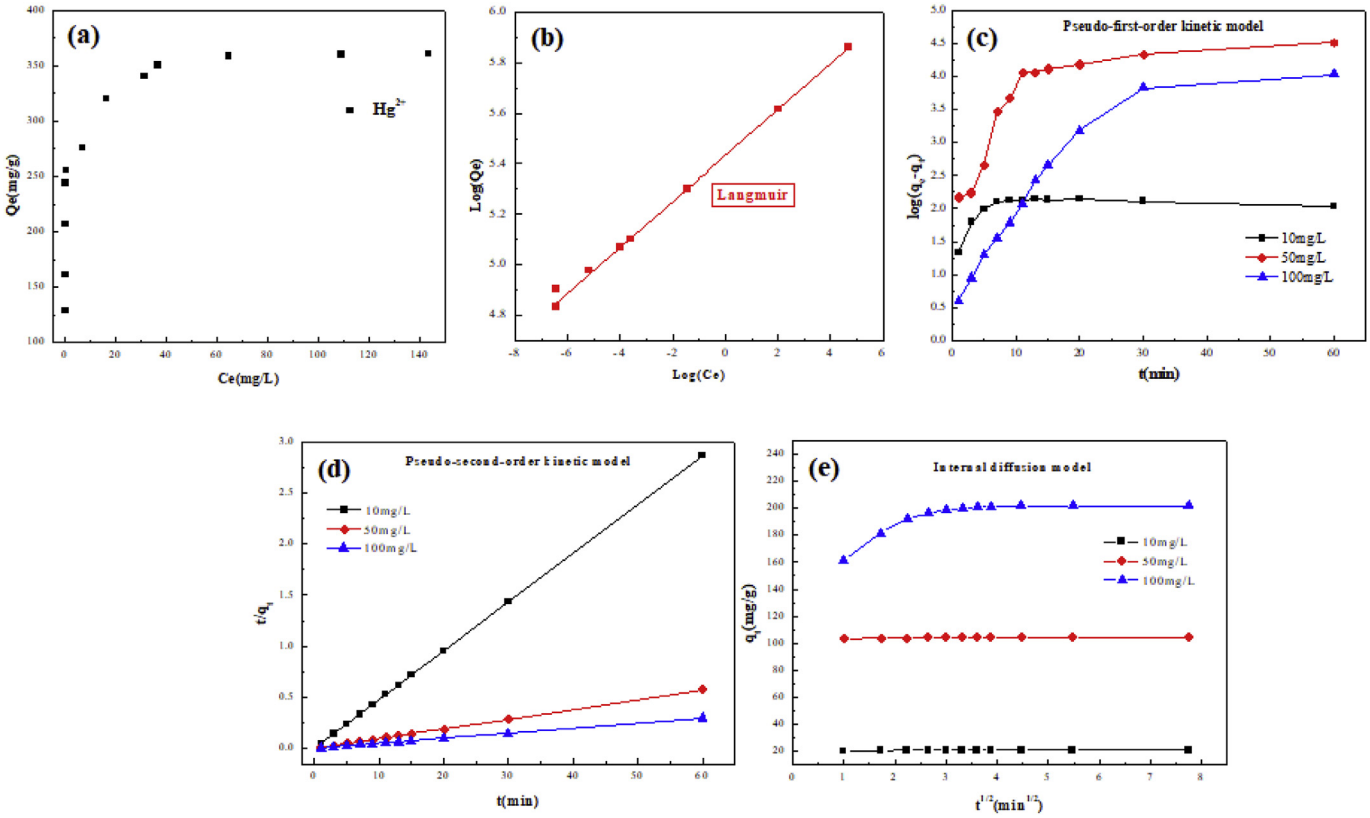

Fig. 4. Adsorption isotherm and kinetics of $[SnS_4]^{4-}$ cluster modified MgAl-LDH composite for Hg^{2+} (a) Experimental data (b) Linear regression by fitting the data with Langmuir adsorption model; and (c) Pseudo-first-order kinetic model, (d) Pseudo-second-order kinetic model, and (e) Internal diffusion model for Hg^{2+} sorption.

respectively; Table S6) (Jawad et al., 2017; Ma et al., 2016; Ma et al., 2014b).

Two classical adsorption models, the Langmuir and Freundlich isotherm models, were used to investigate the adsorption mechanism of mercury ions on $[SnS_4]^{4-}$ cluster modified Mg/Al-LDH composite. The results of date fitting using two classical adsorption model were shown in Fig. 4(b). The adsorption isotherms fitted with Langmuir adsorption model with correlation coefficient of 0.999. Therefore, this indicated that monolayer adsorption was the better form to describe the adsorption behavior of Hg^{2+} in the layered structure of $[SnS_4]^{4-}$ cluster modified MgAl-LDH composite.

As depicted in Fig. 4(c) and (d), adsorption behaviors were determined by fitting two different kinetic models. It is obvious that the pseudo-second-order kinetics model is the best to describe the adsorption of Hg^{2+} by $[SnS_4]^{4-}$/MgAl-LDH composite, with fit coefficient of 1.0. The internal diffusion model is used to analyze the control steps in the reaction. Fig. 4(e) shown that at low Hg^{2+} concentration (10 and 50 mg L^{-1}), the adsorption equilibrium was reached quickly (within 1 $min^{0.5}$), while at 100 mg L^{-1}, the adsorption equilibrium was reached only after 3 $min^{0.5}$ or so. So we postulated that fast film diffusion is the rate control process at low Hg^{2+} concentration. While, at high Hg^{2+} concentration, the beginning of the adsorption is a fast film diffusion process, the second linear section is a slow pore diffusion which is the process of rate control, and the third section is the final equilibrium stage where the internal diffusion begins to weaken due to the decrease in the concentration of mercury ions. Therefore, the internal diffusion wasn't controlled by a single rate during mercury adsorption process. Meanwhile, even at three different initial Hg^{2+} concentrations, the calculated adsorption capacities according to the pseudo-second-order model were almost the same. Therefore, investigations on these adsorption kinetics parameters revealed that the adsorption process for Hg^{2+} onto adsorbent was more likely to be a chemisorption.

3.3.2. *Adsorption mechanism for Hg^{2+} uptake*

It was found that the color of the composite turned to faint yellow immediately after the $[SnS_4]^{4-}$/MgAl-LDH sorbent was added into the solution. Then the $[SnS_4]^{4-}$/MgAl-LDH sorbent turned to dark green after 30 min reaction. It further indicated that it is a chemical-adsorption process. The XPS analysis for S 2p and Hg 4f is shown in Fig. 5. As shown in Fig. 5(a) and (b), for the S 2p of fresh and used adsorbents, peaks at 167.0–169.0 eV were corresponded to surface sulfate, and peaks at 161.0–163.0 eV were assigned to poly sulfur. For fresh sample, the ratio of surface sulfate to poly sulfur was 1.155. However, the ratio of surface sulfate to poly sulfur increased to 2.268 after adsorbing Hg^{2+} because SO_4^{2-} from the $HgSO_4$ solution entered into the interlayer of the adsorbent. For Hg 4f in Fig. 5(c), the peaks at 103.8 eV and 99.8 eV were assigned to Hg 4f 5/2 and 4f 7/2 energies of Hg^{2+}, respectively, demonstrating the capture of Hg^{2+}. Additionally, as shown in Fig. S8 and Fig. S9, Mg and Al in $[SnS_4]^{4-}$/MgAl-LDH also appeared with binding energies of 1304.50–1304.60 eV and 74.42–74.53 eV in both fresh and spent materials, respectively, which supported the stability of $[SnS_4]^{4-}$/MgAl-LDH. Moreover, a new distinct basal spacing at 0.930 nm in the XRD patterns of used $[SnS_4]^{4-}$/MgAl-LDH (Fig. 1) might be attributed to the coordination of mercury ions with $[SnS_4]^{4-}$ clusters. Likewise, the FT-IR spectra of used $[SnS_4]^{4-}$/MgAl-LDH (Fig. S1) showed an obvious prominent peak (at ca. 1100 cm^{-1}), providing further evidence of sulfate ion intercalation during adsorption to balance the charge of mercury ions (Radha et al., 2007). Thus, when Hg^{2+} concentration is lower than that required to saturate the

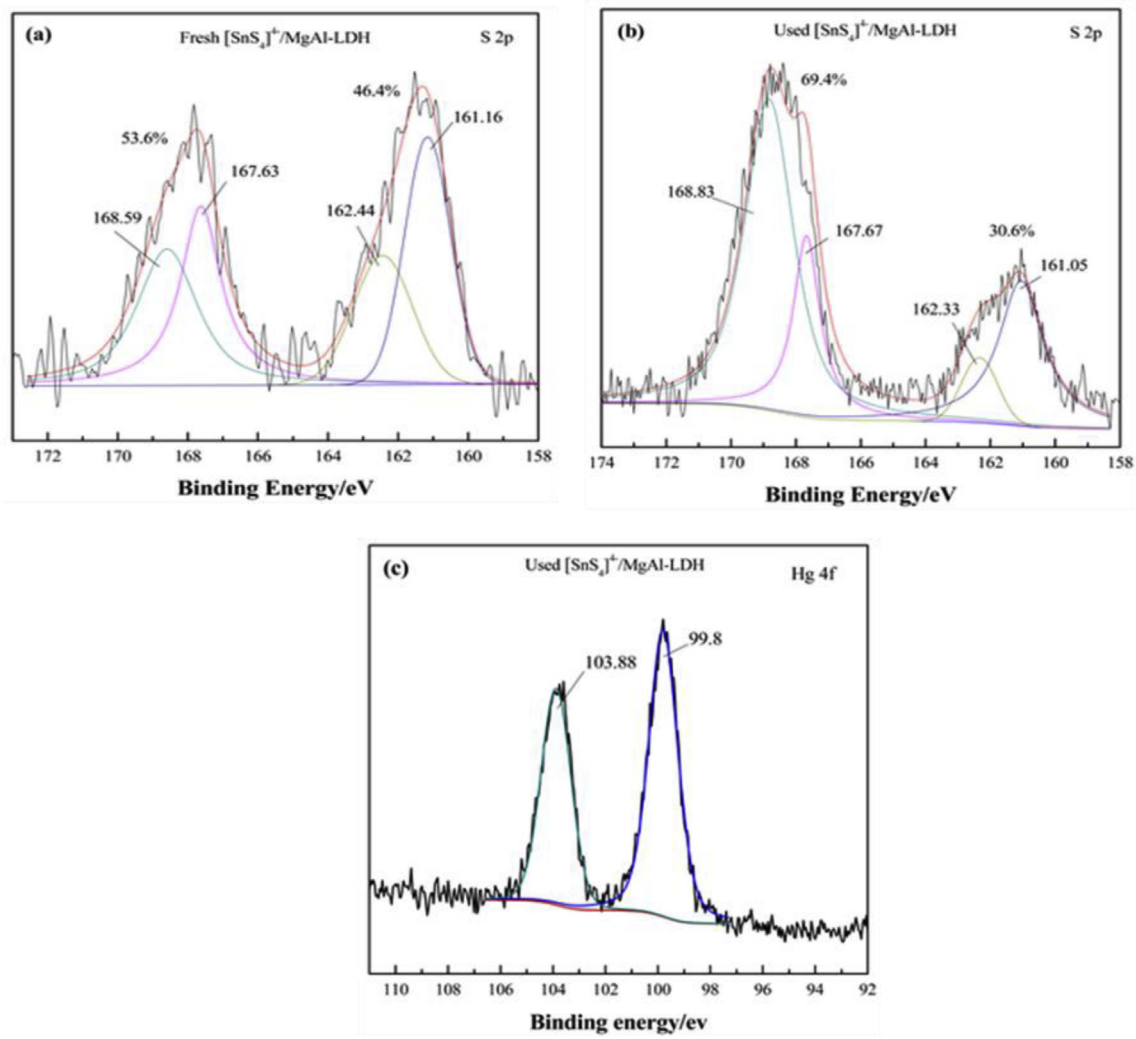

Fig. 5. XPS survey spectrum for S 2p and Hg 4f. (a) corresponds to adsorbent before adsorption; (b) and (c) are those after mercury adsorption.

sorbent, the capture could be described by eq (9):

$$\text{LDH-}[(SnS_4)^{4-}] + HgSO_4 \rightarrow \text{LDH-}[Hg_2(SnS_4)]^{4-}(SO_4^{2-})_2 \quad (9)$$

To explore the mechanism in case of mercury ions being in excess, seven kinds of as-prepared adsorbents with different $[SnS_4]^{4-}$ content were used to complete adsorption saturation experiment. As shown in Table S7, molar ratios of Hg^{2+} and $[SnS_4]^{4-}$ calculated from the saturated adsorption capacities were close to 2.0. In this case, adsorption mechanism probably corresponded with eq (10):

$$\text{LDH-}[(SnS_4)^{4-}] + HgSO_4 \rightarrow Hg_2(SnS_4) + \text{LDH-}SO_4 \quad (10)$$

Based on the above discussion, as Fig. 6 illustrated, $[SnS_4]^{4-}$ clusters were grown into the layered structure of MgAl-LDH through ion-exchange. The surface area was enlarged which benefitted the adsorption reaction. Proposed adsorption mechanism of $[SnS_4]^{4-}$/MgAl-LDH for Hg^{2+} was relatively complex chemical adsorption.

3.4. Recycle of the adsorbents

Suitable disposal of a spent sorbents is of significance for avoiding secondary pollution. The sorbent after Hg^{2+} absorption was immersed in Na_2S solution (1 M) and the solution had been light in color in seconds (Fig. S10). Chemical analysis demonstrates that the adsorbent contains only 0.048% mercury after being treated by Na_2S solution for 1 h, thus realizing the recycling of adsorbents. Therefore, it was efficient and safe to apply $[SnS_4]^{4-}$/MgAl-LDH for Hg^{2+} removal in fouling acid wastewater.

4. Conclusions

The $[SnS_4]^{4-}$/MgAl-LDH composite was prepared through an ion-exchange method between MgAl-LDH and $[SnS_4]^{4-}$ clusters. $[SnS_4]^{4-}$ clusters were indicated to have strong affinity toward Hg^{2+} ions and $HgSO_4$ molecule. The adsorption process was weakly affected by the initial concentration of mercury but strongly influenced by the solution pH, and the lower pH value is more favorable for Hg^{2+} removal. Based on the mechanism study, the chemical adsorption process attributed the high Hg^{2+} removal efficiency, with the new product of $Hg_2(SnS_4)$. Langmuir isotherm model fitted well with the experimental data. Isotherms and kinetics studies showed that the adsorption profiles of prepared adsorbents followed a monolayer chemical adsorption model. Such novel materials exhibited a potential possibility for the application of mercury uptake from acid wastewater.

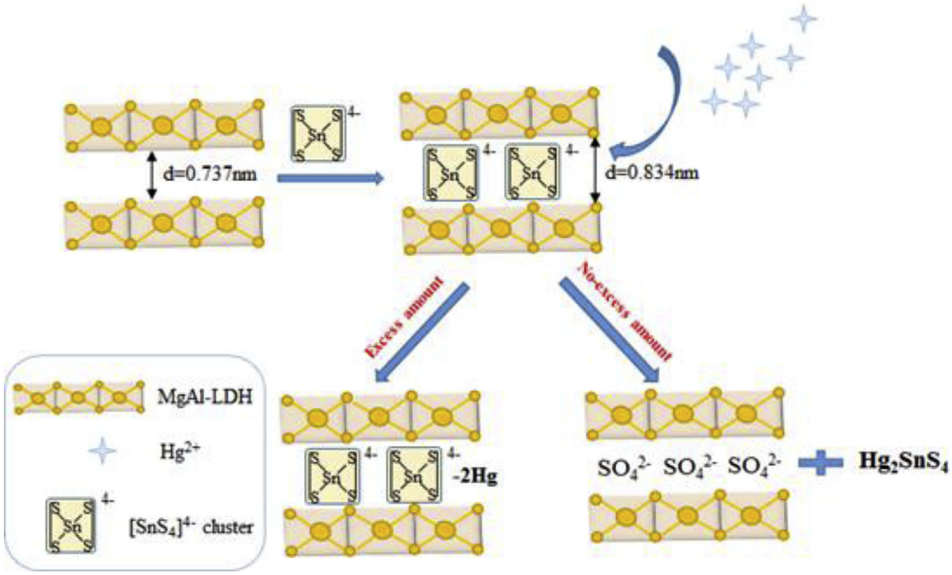

Fig. 6. The proposed Hg^{2+} removal mechanism over $[SnS_4]^{4-}$/MgAl-LDH composite.

Acknowledgements

This study was supported by the National Key R&D Program of China (2017YFC0210500) and the National Natural Science Foundation of China (No. 21806105, No.21677096 and No.21607102). This study was also supported by National Postdoctoral Program for Innovative Talents (No.BX201700151). Thanks for the support of China's Post-doctoral Science Fun (No. 2017M620156).

Appendix A. Supplementary data

The tables for kinetic study for Hg^{2+} under excess of amount, BET of as-prepared materials, Hg^{2+} and Sn^{2+} concentrations of solution in the mercury removal process, the concentrations of Sn^{2+}, S^{2-}, Mg^{2+} and Al^{3+} before and after treatment with HCl solution, and comparison of adsorption capacity for Hg^{2+} with adsorbents in literature. And the figures for the influence of ratio between $[SnS_4]^{4-}$ cluster and MgAl-LDH, influence of different mercury compounds dissolved in different acid solution, the removal efficiency of Cu^{2+}, Pb^{2+}, Cr^{3+}, Cd^{2+}, Zn^{2+}, Ni^{2+} and Co^{2+}, respectively, SEM, TEM (including EDX) analysis and FT-IR spectra of sample, XPS of Mg and Al, and photos of the process of mercury recycling are put in supporting information.

Supplementary data to this article can be found online at https://doi.org/10.1016/j.envpol.2018.12.009.

References

Abu-Danso, E., Peraniemi, S., Leiviska, T., Bhatnagar, A., 2018. Synthesis of S-ligand tethered cellulose nanofibers for efficient removal of Pb(II) and Cd(II) ions from synthetic and industrial wastewater. Environ. Pollut. 242, 1988–1997.
Alcázar, Á., Garrido, I., García, E.M., de Lucas, A., Carmona, M., Rodriguez, J.F., 2015. New type of highly selective microcapsules for the removal of mercury from surface polluted waters. Separ. Purif. Technol. 154, 255–262.
Ali, S.A., Mazumder, M.A.J., 2018. A new resin embedded with chelating motifs of biogenic methionine for the removal of Hg (II) at ppb levels. J. Hazard Mater. 350, 169–179.
Amiri, M.J., Arshadi, M., Giannakopoulos, E., Kalavrouziotis, I.K., 2018. Removal of mercury (II) and lead (II) from aqueous media by using a green adsorbent: kinetics, thermodynamic, and mechanism studies. J. Hazard Toxic Radioact Waste. 22, 04017026.
K, K., Rangan, P.N., Trikalitis, C.C., 2002. Hexagonal pore organization in mesostructured metal tin sulfides built with $[Sn_2S_6]^{4-}$ cluster. Nano Lett. 2, 513–517.
Barth, B.E., Leusmann, E., Harms, K., Dehnen, S., 2013. Towards the installation of transition metal ions on donor ligand decorated tin sulfide clusters. Chem. Commun. 49, 6590–6592.
Borreguero, A.M., Leura, A., Rodríguez, J.F., Vaselli, O., Nisi, B., Higueras, P.L., Carmona, M., 2018. Modelling the mercury removal from polluted waters by using TOMAC microcapsules considering the metal speciation. Chem. Eng. J. 341, 308–316.
Chu, L., Liu, C., Zhou, G., Xu, R., Tang, Y., Zeng, Z., Luo, S., 2015. A double network gel as low cost and easy recycle adsorbent: highly efficient removal of Cd (II) and Pb (II) pollutants from wastewater. J. Hazard. Mater. 300, 153–160.
Coleman, R., Colley, J., Klausmeier, R., Meserole, N., Micheletti, W., 1980. Sources and Treatment of Wastewater in the Nonferrous Metals Industry.
Fakhri, A., 2015. Investigation of mercury (II) adsorption from aqueous solution onto copper oxide nanoparticles: optimization using response surface methodology. Process Saf. Environ. Protect. 93, 1–8.
Fang, L., Li, L., Qu, Z., Xu, H., Xu, J., Yan, N., 2018. A novel method for the sequential removal and separation of multiple heavy metals from wastewater. J. Hazard Mater. 342, 617–624.
Gong, Y., Liu, Y., Xiong, Z., Kaback, D., Zhao, D., 2012. Immobilization of mercury in field soil and sediment using carboxymethyl cellulose stabilized iron sulfide nanoparticles. Nanotechnology 23, 1–13.
Gong, Y., Liu, Y., Xiong, Z., Zhao, D., 2014. Immobilization of mercury by carboxymethyl cellulose stabilized iron sulfide nanoparticles: reaction mechanisms and effects of stabilizer and water chemistry. Environ. Sci. Technol. 48, 3986–3994.
Gonzalez Rodriguez, P., de Ruiter, M., Wijnands, T., Ten Elshof, J.E., 2017. Porous layered double hydroxides synthesized using oxygen generated by decomposition of hydrogen peroxide. Sci. Rep. 7, 1–9.
Gu, P., Zhang, S., Li, X., Wang, X., Wen, T., Jehan, R., Alsaedi, A., Hayat, T., Wang, X., 2018. Recent advances in layered double hydroxide-based nanomaterials for the removal of radionuclides from aqueous solution. Environ. Pollut. 240, 493–505.
Hafeznezami, S., Zimmer-Faust, A.G., Dunne, A., Tran, T., Yang, C., Lam, J.R., Reynolds, M.D., Davis, J.A., Jay, J.A., 2016. Adsorption and desorption of arsenate on sandy sediments from contaminated and uncontaminated saturated zones: kinetic and equilibrium modeling. Environ. Pollut. 215, 290–301.
Hargreaves, A.J., Vale, P., Whelan, J., Constantino, C., Dotro, G., Cartmell, E., 2016. Mercury and antimony in wastewater: fate and treatment. Water Air Soil Pollut. 227, 1–17.
Hassan, S.S.M., Kamel, A.K., Awwad, N.S., Aboterika, A.H.A., Yahia, I.S., 2018. Adsorbent for efficient removal of mercury(Ii) from aqueous solution. Europ. Chem. Bulletin 6, 558–563.
Jawad, A., Liao, Z., Zhou, Z., Khan, A., Wang, T., Ifthikar, J., Shahzad, A., Chen, Z., Chen, Z., 2017. Fe-MoS_4: an effective and stable LDH-based adsorbent for selective removal of heavy metals. ACS Appl. Mater. Interfaces 9, 28451–28463.
Jia, F., Wang, Q., Wu, J., Li, Y., Song, S., 2017. Two-dimensional molybdenum disulfide as a superb adsorbent for removing Hg^{2+} from water. ACS Sustain. Chem. Eng. 5, 7410–7419.
Ke, J., Li, X., Shi, Y., Zhao, Q., Jiang, X., 2012. A facile and highly sensitive probe for Hg(II) based on metal-induced aggregation of ZnSe/ZnS quantum dots. Nanoscale 4, 4996–5001.
Kumari, R., 2011. Preliminary mercury emission estimates from non–ferrous metal smelting in India. Atmos. Pollution Res. 2, 513–519.
Lei, C., Zhu, X., Zhu, B., Jiang, C., Le, Y., Yu, J., 2017. Superb adsorption capacity of

hierarchical calcined Ni/Mg/Al layered double hydroxides for Congo red and Cr(VI) ions. J. Hazard Mater. 321, 801–811.
Li, Y., Du, Q., Wang, X., Zhang, P., Wang, D., Wang, Z., Xia, Y., 2010. Removal of lead from aqueous solution by activated carbon prepared from Enteromorpha prolifera by zinc chloride activation. J. Hazard Mater. 183, 583–589.
Ma, S., Chen, Q., Li, H., Wang, P., Islam, S.M., Gu, Q., Yang, X., Kanatzidis, M.G., 2014a. Highly selective and efficient heavy metal capture with polysulfide intercalated layered double hydroxides. J. Mater. Chem. 2, 10280–10289.
Ma, Y., Qu, Z., Xu, H., Wang, W., Yan, N., 2014b. Investigation on mercury removal method from flue gas in the presence of sulfur dioxide. J. Hazard Mater. 279, 289–295.
Ma, L., Wang, Q., Islam, S.M., Liu, Y., Ma, S., Kanatzidis, M.G., 2016. Highly selective and efficient removal of heavy metals by layered double hydroxide intercalated with the MoS_4^{2-}ion. J. Am. Chem. Soc. 138, 2858–2866.
Ma, L., Islam, S.M., Xiao, C., Zhao, J., Liu, H., Yuan, M., Sun, G., Li, H., Ma, S., Kanatzidis, M.G., 2017. Rapid simultaneous removal of toxic anions $[HSeO_3]^-$, $[SeO_3]^{2-}$, and $[SeO_4]^{2-}$, and metals Hg^{2+}, Cu^{2+}, and Cd^{2+} by MoS_4^{2-} intercalated layered double hydroxide. J. Am. Chem. Soc. 139, 12745–12757.
Muliwa, A.M., Onyango, M.S., Maity, A., Ochieng, A., 2017. Batch equilibrium and kinetics of mercury removal from aqueous solutions using polythiophene/graphene oxide nanocomposite. Water Sci. Technol. 75, 2841–2851.
Oh, Y., Bag, S., Malliakas, C.D., Kanatzidis, M.G., 2011. Selective surfaces: high-surface-area zinc tin sulfide chalcogels. Chem. Mater. 23, 2447–2456.
Qu, Z., Yan, L., Li, L., Xu, J., Liu, M., Li, Z., Yan, N., 2014. Ultraeffective ZnS nanocrystals sorbent for mercury(II) removal based on size-dependent cation exchange. ACS Appl. Mater. Interfaces 6, 18026–18032.
Radha, A., Kamath, P.V., Shivakumara, C., 2007. Conservation of order, disorder, and "crystallinity" during anion-exchange reactions among layered double hydroxides (LDHs) of Zn with Al. J. Phys. Chem. B 111, 3411–3418.
Sajjadi, S.-A., Mohammadzadeh, A., Tran, H.N., Anastopoulos, I., Dotto, G.L., Lopičić, Z.R., Sivamani, S., Rahmani-Sani, A., Ivanets, A., Hosseini-Bandegharaei, A., 2018. Efficient mercury removal from wastewater by pistachio wood wastes-derived activated carbon prepared by chemical activation using a novel activating agent. J. Environ. Manag. 223, 1001–1009.
Shadbad, M.J., Mohebbi, A., Soltani, A., 2011. Mercury (II) removal from aqueous solutions by adsorption on multi-walled carbon nanotubes. Kor. J. Chem. Eng. 28, 1029–1034.
Shafaei-Fallah, M., Rothenberger, A., Katsoulidis, A.P., He, J., Malliakas, C.D., Kanatzidis, M.G., 2011. Extraordinary selectivity of $CoMo_3S_{13}$ chalcogel for C_2H_6 and CO_2 adsorption. Adv. Mater. 23, 4857–4860.
Shim, Y., Yuhas, B.D., Dyar, S.M., Smeigh, A.L., Douvalis, A.P., Wasielewski, M.R., Kanatzidis, M.G., 2013. Tunable biomimetic chalcogels with Fe_4S_4 cores and $[Sn_nS_{2n+2}]^{4-}$(n = 1, 2, 4) building blocks for solar fuel catalysis. J. Am. Chem. Soc. 135, 2330–2337.
Sun, M., Hou, J., Cheng, G., Baig, S.A., Tan, L., Xu, X., 2014. The relationship between speciation and release ability of mercury in flue gas desulfurization (FGD) gypsum. Fuel 125, 66–72.
Sun, Y., Lv, D., Zhou, J., Zhou, X., Lou, Z., Baig, S.A., Xu, X., 2017. Adsorption of mercury (II) from aqueous solutions using FeS and pyrite: a comparative study. Chemosphere 185, 452–461.
Tahmasebi, E., Masoomi, M.Y., Yamini, Y., Morsali, A., 2014. Application of mechanosynthesized azine-decorated zinc (II) metal–organic frameworks for highly efficient removal and extraction of some heavy-metal ions from aqueous samples: a comparative study. Inorg. Chem. 54, 425–433.
Trasande, L., DiGangi, J., Evers, D.C., Petrlik, J., Buck, D.G., Šamánek, J., Beeler, B., Turnquist, M.A., Regan, K., 2016. Economic implications of mercury exposure in the context of the global mercury treaty: hair mercury levels and estimated lost economic productivity in selected developing countries. J. Environ. Manag. 183, 229–235.
United Nations Environment Programme (UNEP). Global Mercury Assessment 2013: Sources, Emissions, Releases and Environmental Transport. UNEP Chemicals Branch, Geneva, Switzerland.
Xu, H., Xie, J., Ma, Y., Qu, Z., Zhao, S., Chen, W., Huang, W., Yan, N., 2015. The cooperation of FeSn in a MnOx complex sorbent used for capturing elemental mercury. Fuel 140, 803–809.
Xu, J., Qu, Z., Yan, N., Zhao, Y., Xu, X., Li, L., 2016a. Size-dependent nanocrystal sorbent for copper removal from water. Chem. Eng. J. 284, 565–570.
Xu, X., Schierz, A., Xu, N., Cao, X., 2016b. Comparison of the characteristics and mechanisms of Hg (II) sorption by biochars and activated carbon. J. Colloid Interface Sci. 463, 55–60.
Xu, W., Hussain, A., Liu, Y., 2018. A review on modification methods of adsorbents for elemental mercury from flue gas. Chem. Eng. J. 346, 692–711.
Xue, T., Kun, L., Han, Y., Hu, Y., Aimin, L., 2016. Simultaneous removal of acid green 25 and mercury ions from aqueous solutions using glutamine modified chitosan magnetic composite microspheres. Environ. Pollut. 209, 21–29.
Yu, S., Liu, Y., Ai, Y., Wang, X., Zhang, R., Chen, Z., Chen, Z., Zhao, G., Wang, X., 2018. Rational design of carbonaceous nanofiber/Ni-Al layered double hydroxide nanocomposites for high-efficiency removal of heavy metals from aqueous solutions. Environ. Pollut. 242, 1–11.
Yuhas, B.D., Smeigh, A.L., Samuel, A.P., Shim, Y., Bag, S., Douvalis, A.P., Wasielewski, M.R., Kanatzidis, M.G., 2011. Biomimetic multifunctional porous chalcogels as solar fuel catalysts. J. Am. Chem. Soc. 133, 7252–7255.
Zhang, B., Dong, Z., Sun, D., Wu, T., Li, Y., 2017. Enhanced adsorption capacity of dyes by surfactant-modified layered double hydroxides from aqueous solution. J. Ind. Eng. Chem. 49, 208–218.
Zhang, H., Jiaqing, W., Zhou, B., Zhou, Y., Dai, Z., Zhou, Q., Chriestie, P., Luo, Y., 2018. Enhanced adsorption of oxytetracycline to weathered microplastic polystyrene: kinetics, isotherms and influencing factors. Environ. Pollut. 243, 1550–1557.
Zhao, D., Yu, Y., Chen, J.P., 2016. Treatment of lead contaminated water by a PVDF membrane that is modified by zirconium, phosphate and PVA. Water Res. 101, 564–573.
Zhi, L., Zuo, W., Chen, F., Wang, B., 2016. 3D MoS_2 composition aerogels as chemosensors and adsorbents for colorimetric detection and high-capacity adsorption of Hg^{2+}. ACS Sustain. Chem. Eng. 4, 3398–3408.